Photonic crystals and optical mode engineering for thin film photovoltaics

Guillaume Gomard, Romain Peretti, Emmanuel Drouard, Xianqin Meng, C. Seassal

Photonic crystals and optical mode engineering for thin film photovoltaics

Guillaume Gomard, [1,2] Romain Peretti, [1] Emmanuel Drouard, [1] Xianqin Meng, [1,2] and Christian Seassal [1,*]

Université de Lyon, Institut des Nanotechnologies de Lyon (INL) UMR 5270 CNRS-INSA-ECL-UCBL, France
[1]Ecole Centrale de Lyon, 36 avenue Guy de Collongue, 69134, Ecully Cedex, France
[2]INSA de Lyon, Bat. Blaise Pascal, 7 avenue Jean Capelle, 69621, Villeurbanne, France
[*]christian.seassal@ec-lyon.fr

Abstract: In this paper, we present the design, analysis, and experimental results on the integration of 2D photonic crystals in thin film photovoltaic solar cells based on hydrogenated amorphous silicon. We introduce an analytical approach based on time domain coupled mode theory to investigate the impact of the photon lifetime and anisotropy of the optical resonances on the absorption efficiency. Specific design rules are derived from this analysis. We also show that, due to the specific properties of the photonic crystal resonances, the angular acceptance of such solar cells is particularly high. Rigorous Coupled Wave Analysis simulations show that the absorption in the a-Si:H active layers, integrated from 300 to 750nm, is only decreased from 65.7% to 60% while the incidence angle is increased from 0 to 55°. Experimental results confirm the stability of the incident light absorption in the patterned stack, for angles of incidence up to 50°.

OCIS codes: (350.6050) Solar energy; (040.5350) Photovoltaic; (050.5298) Photonic crystals.

References and links

1. A. Naqavi, F.-J. Haug, C. Battaglia, H. P. Herzig, and C. Ballif, "Light trapping in solar cells at the extreme coupling limit," J. Opt. Soc. Am. B **30**(1), 13–20 (2013).
2. Z. Yu, A. Raman, and S. Fan, "Thermodynamic upper bound on broadband light coupling with photonic structures," Phys. Rev. Lett. **109**(17), 173901 (2012).
3. P. Bermel, C. Luo, L. Zeng, L. C. Kimerling, and J. D. Joannopoulos, "Improving thin-film crystalline silicon solar cell efficiencies with photonic crystals," Opt. Express **15**(25), 16986–17000 (2007).
4. R. Bouffaron, L. Escoubas, J. J. Simon, P. Torchio, F. Flory, G. Berginc, and P. Masclet, "Enhanced antireflecting properties of micro-structured top-flat pyramids," Opt. Express **16**(23), 19304–19309 (2008).
5. Y. M. Song, S. J. Jang, J. S. Yu, and Y. T. Lee, "Bioinspired parabola subwavelength structures for improved broadband antireflection," Small **6**(9), 984–987 (2010).
6. H. A. Atwater and A. Polman, "Plasmonics for improved photovoltaic devices," Nat. Mater. **9**(3), 205–213 (2010).
7. M. Despeisse, C. Battaglia, M. Boccard, G. Bugnon, M. Charrière, P. Cuony, S. Hänni, L. Löfgren, F. Meillaud, G. Parascandolo, T. Söderström, and C. Ballif, "Optimization of thin film silicon solar cells on highly textured substrates," Phys. Status Solidi A **208**(8), 1863–1868 (2011).
8. C. Battaglia, C.-M. Hsu, K. Söderström, J. Escarré, F.-J. Haug, M. Charrière, M. Boccard, M. Despeisse, D. T. L. Alexander, M. Cantoni, Y. Cui, and C. Ballif, "Light trapping in solar cells: Can periodic beat random?" ACS Nano **6**(3), 2790–2797 (2012).
9. M. G. Deceglie, V. E. Ferry, A. P. Alivisatos, and H. A. Atwater, "Design of nanostructured solar cells using coupled optical and electrical modeling," Nano Lett. **12**(6), 2894–2900 (2012).
10. C. Seassal, Y. Park, A. Fave, E. Drouard, E. Fourmond, A. Kaminski, M. Lemiti, X. Letartre, and P. Viktorovitch, "Photonic crystal assisted ultra-thin silicon photovoltaic solar cell," Proc. SPIE **7002**, 700207, 700207-8 (2008).
11. D. Duché, L. Escoubas, J.-J. Simon, P. Torchio, W. Vervisch, and F. Flory, "Slow bloch modes for enhancing the absorption of light in thin films for photovoltaic cells," Appl. Phys. Lett. **92**(19), 193310 (2008).
12. Y. Park, E. Drouard, O. El Daif, X. Letartre, P. Viktorovitch, A. Fave, A. Kaminski, M. Lemiti, and C. Seassal, "Absorption enhancement using photonic crystals for silicon thin film solar cells," Opt. Express **17**(16), 14312–14321 (2009).
13. S. Zanotto, M. Liscidini, and L. C. Andreani, "Light trapping regimes in thin-film silicon solar cells with a photonic pattern," Opt. Express **18**(5), 4260–4274 (2010).

#183852 - $15.00 USD Received 4 Feb 2013; revised 17 Mar 2013; accepted 18 Mar 2013; published 22 Apr 2013

14. G. Gomard, X. Meng, E. Drouard, K. E. Hajjam, E. Gerelli, R. Peretti, A. Fave, R. Orobtchouk, M. Lemiti, and C. Seassal, "Light harvesting by planar photonic crystals in solar cells: the case of amorphous silicon," J. Opt. **14**(2), 024011 (2012).
15. G. Gomard, E. Drouard, X. Letartre, X. Meng, A. Kaminski, A. Fave, M. Lemiti, E. Garcia-Caurel, and C. Seassal, "Two-dimensional photonic crystal for absorption enhancement in hydrogenated amorphous silicon thin film solar cells," J. Appl. Phys. **108**(12), 123102 (2010).
16. H. A. Haus, *Waves and Fields in Optoelectronics* (Englewood Cliffs, 1984).
17. Z. Yu, A. Raman, and S. Fan, "Fundamental limit of light trapping in grating structures," Opt. Express **18**(S3 Suppl 3), A366–A380 (2010).
18. Z. Yu, A. Raman, and S. Fan, "Nanophotonic light-trapping theory for solar cells," Appl. Phys., A Mater. Sci. Process. **105**(2), 329–339 (2011).
19. Z. Yu, A. Raman, and S. Fan, "Fundamental limit of nanophotonic light trapping in solar cells," Proc. Natl. Acad. Sci. U.S.A. **107**(41), 17491–17496 (2010).
20. R. Peretti, G. Gomard, C. Seassal, X. Letartre, and E. Drouard, "Modal approach for tailoring the absorption in a photonic crystal membrane," J. Appl. Phys. **111**(12), 123114 (2012).
21. C. Manolatou, M. Khan, S. Fan, P. Villeneuve, H. Haus, and J. Joannopoulos, "Coupling of modes analysis of resonant channel add-drop filters," IEEE J. Quantum Electron. **35**(9), 1322–1331 (1999).
22. S. B. Mallick, M. Agrawal, and P. Peumans, "Optimal light trapping in ultra-thin photonic crystal crystalline silicon solar cells," Opt. Express **18**(6), 5691–5706 (2010).
23. L. Li, K.-Q. Peng, B. Hu, X. Wang, Y. Hu, X.-L. Wu, and S.-T. Lee, "Broadband optical absorption enhancement in silicon nanofunnel arrays for photovoltaic applications," Appl. Phys. Lett. **100**(22), 223902 (2012).
24. V. Mandelshtam, "Fdm: the filter diagonalization method for data processing in nmr experiments," Prog. Nucl. Magn. Reson **38**(2 Spec.), 159–196 (2001).
25. A. Oskooi, P. A. Favuzzi, Y. Tanaka, H. Shigeta, Y. Kawakami, and S. Noda, "Partially disordered photonic-crystal thin films for enhanced and robust photovoltaics," Appl. Phys. Lett. **100**(18), 181110 (2012).
26. E. R. Martins, J. Li, Y. Liu, J. Zhou, and T. F. Krauss, "Engineering gratings for light trapping in photovoltaics: The supercell concept," Phys. Rev. B **86**(4), 041404 (2012).
27. K. Vynck, M. Burresi, F. Riboli, and D. S. Wiersma, "Photon management in two-dimensional disordered media," Nat. Mater. **11**(12), 1017–1022 (2012).
28. A. Bozzola, M. Liscidini, and L. C. Andreani, "Photonic light-trapping versus Lambertian limits in thin film silicon solar cells with 1D and 2D periodic patterns," Opt. Express **20**(S2 Suppl 2), A224–A244 (2012).
29. X. Meng, V. Depauw, G. Gomard, O. El Daif, C. Trompoukis, E. Drouard, C. Jamois, A. Fave, F. Dross, I. Gordon, and C. Seassal, "Design, fabrication and optical characterization of photonic crystal assisted thin film monocrystalline-silicon solar cells," Opt. Express **20**(S4 Suppl 4), A465–A475 (2012).
30. C. Trompoukis, O. El Daif, V. Depauw, I. Gordon, and J. Poortmans, "Photonic assisted light trapping integrated in ultrathin crystalline silicon solar cells by nanoimprint lithography," Appl. Phys. Lett. **101**(10), 103901 (2012).
31. K. Sakoda, *Optical Properties of Photonic Crystals* (Springer, 2001), vol. 80.

1. Introduction

The recent development of nanophotonics has triggered the emergence of novel concepts for light management in photovoltaic solar cells. This includes incident light trapping and strategies to control light absorption in thin film solar cells. The interest of the whole range of accessible nanophotonic structures has been considered by an increasing number of research groups during the past years (see e.g [1,2].).

Periodic dielectric structures like diffraction gratings positioned at the back of solar cells appear promising to increase the photon path length, especially for high wavelengths, i.e. when the absorption of the active material is low [3]. On the top of the devices, novel anti-reflecting structures have been proposed, based on the integration of sub-wavelength structures with a large range of shapes [4,5], up to complex multi-scale biomimetic structures. On the other hand the use of plasmonic resonances to control light capture and absorption by scattering or near field enhancement has been proposed by many groups (see e.g [6].). In particular, various ways to implement such light trapping strategies on solar cells based on hydrogenated amorphous silicon (a-Si:H), have been introduced during the past years. Most approaches rely on the deposition of more or less conformal layers onto a patterned substrate [7–9]. Using an efficient light trapping strategy on such a-Si:H-based devices appears particularly relevant since it could lead to a high absorption level, while reducing the active layer thickness, and therefore the impact of bulk carrier recombination.

Although all these approaches are promising and could end up in a real increase of the conversion efficiency, sometimes larger than the one calculated considering the lambertian limit, a more in-depth modification of the optical properties of the absorber is needed if one

#183852 - $15.00 USD Received 4 Feb 2013; revised 17 Mar 2013; accepted 18 Mar 2013; published 22 Apr 2013

wishes to drastically reduce the thickness of the solar cell, and therefore its cost, or to significantly increase its efficiency. To reach this goal, photonic crystals (PhC) may offer their wide variety of optical modes, including slow light or Fano-like resonances, while they do not suffer from the parasitic absorption of metallic nanostructures. In 2008, a novel approach was proposed to reach an in-depth modification of the optical density of state, thanks to the use of slow light Bloch modes standing over the light line of PhC. This is achieved by patterning the absorbing layer itself as a planar 1D or 2D PhC [10–13]. If all kinds of absorbing materials could be patterned as such structures, it appears more beneficial in the case of inorganic solar cells, where the refractive indices of the active materials are much higher than in the organic case. Indeed, it has been shown both theoretically and experimentally that incident light absorption in a 100nm thick layer of a-Si:H can be increased by a factor of 2 by the sole impact of the patterning, and in a wavelength range expanding from 300 to 750nm [14]. Moreover, the characteristics of these devices rely on the properties of the multiple Bloch modes of the PhC, which exhibits relatively flat dispersion bands. This is expected to provide a good stability of the device characteristics with regards to the angle of incidence of the sunlight.

In former papers, we have introduced the design of such PhC assisted a-Si:H solar cells [15]. Using Rigorous Coupled Wave Analysis (RCWA), and scanning the main topographical parameters, it is possible to optimize the design of such devices, enabling to increase the integrated absorption in a-Si:H by 27%. Such PhC can be patterned into the active layers of the solar cells, using laser interference lithography and reactive ion etching.

However, while the basic properties of the surface addressable slow light modes are well known, the best way to control them to tailor the absorption over a wide wavelength range is still to be investigated. Indeed, more advanced designs could enable to reach a much higher increase in absorption, and therefore, a substantial increase in terms of conversion efficiency. Moreover, the impact of the unique properties of such Bloch modes on the angular acceptance of PhC solar cells still requires a specific theoretical and experimental investigation.

In this paper we will first introduce the design and basic properties of a-Si:H based PhC assisted solar cells. Then, we will present an approach based on the Time Domain Coupled Mode Theory (TDCMT) [16], which enables to define design rules for the PhC structure integrated in the solar cell. The objective is to reach the highest possible absorption over a given wavelength range. Finally, we will discuss on the angular acceptance of a-Si:H PhC solar cells, in relation with their modal properties.

2. Design and basic properties of a-Si:H based photonic crystal assisted solar cells

The targeted devices are based on a thin film solar cell stack, comprising from the back to the front, a silver (Ag) layer deposited on a glass substrate, a transparent and conductive oxide (TCO) layer made of zinc oxide (ZnO), a p-i-n a-Si:H junction, and another TCO layer formed by the deposition of indium tin oxide (ITO), corresponding to the top electrode. The ZnO layer, with a thickness of 100nm, is expected to act as a barrier against the diffusion of Ag in a-Si:H; it may also play a role in maximizing sunlight absorption. The total thickness of the p-i-n junction is 100nm, which is lower than the diffusion length of the minority carriers in a-Si:H. It is chosen in such a way that the bulk recombination of photocarriers in the active layer is minimized. It also reduces the amount of active material used in the device, compared to more standard designs of a-Si:H based solar cells. The top TCO layer thickness of 50nm is chosen in order to limit the absorption in this material. In the approach proposed, the top layers (ITO and a-Si:H) are fully patterned as a PhC. More precisely, it consists in a 2D square lattice of circular holes, as schematized in Fig. 1(a).

#183852 - $15.00 USD Received 4 Feb 2013; revised 17 Mar 2013; accepted 18 Mar 2013; published 22 Apr 2013

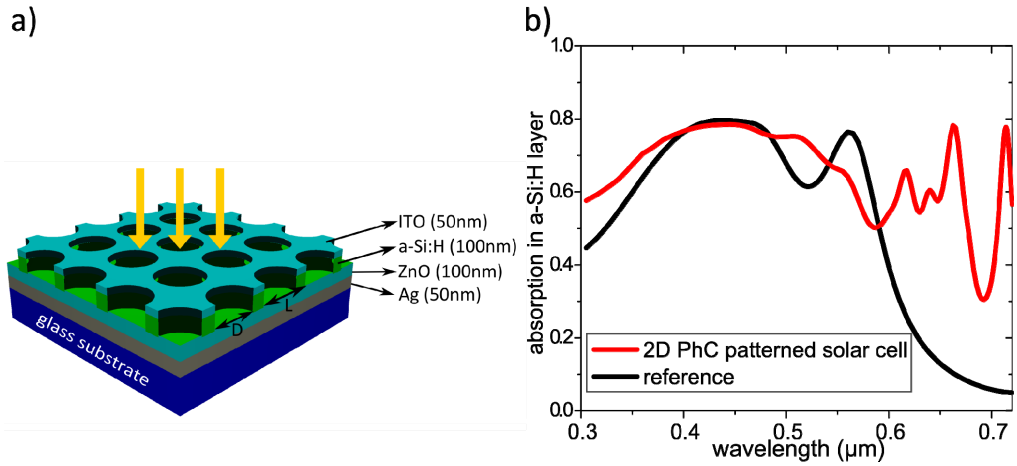

Fig. 1. Schematic view of the 2D PhC assisted a-Si:H solar cells (a), simulated absorption spectra in the active layer for the patterned and for the reference solar cell stacks, both illuminated at normal incidence (b).

Optimizing the lattice parameter, *L*, and the holes diameter, *D*, of the PhC leads to an integrated absorption of 82% in the whole stack, between 300 and 720nm. This value, which is limited to 65.7% if only the useful part of the absorption, namely the one in a-Si:H is considered, is reached for L = 380nm, and D = 237.5nm. Figure 1(b) displays the corresponding absorption spectra for the 2D PhC patterned solar cell and a reference constituted of the same but unpatterned stack, including layers with the same thicknesses. It should be highlighted that this does not correspond to the final optimum for two main reasons. First, only a square lattice of air holes has been considered and second, *L* and *D* are the sole parameters which have been varied in a range limited by fabrication constraints, *L* was tuned in the 200-800nm range, while *D* was varied in order to explore the full range of surfacic air filling fraction from 0 to 1. Still, at this stage, it should be mentioned that this corresponds to a substantial increase with regards to the unpatterned structure, where the absorption in a-Si:H is only of 51.7%. Moreover, the integrated absorption achieved for a PhC solar cell is quite stable with regards to technological uncertainties, since it is only reduced by 1% when *L* or *D* are tuned by 5% from the above-mentioned parameters.

3. Light trapping and absorption in thin film semiconductor solar cell: a physical insight

Most of the approaches which have been proposed to implement light trapping make use of resonant modes to increase the coupling between the incident light and an absorbing layer. To this end, optical simulations are abundantly used to maximize the integrated absorption, simply by systematically scanning a restricted number of free parameters. However, it turns out that the results obtained lack a certain level of physical understanding which enables to make the connection between the absorption enhancement observed and the modal properties involved. If the critical coupling conditions are often mentioned to justify the creation of a new and high absorption peak [14], this explanation is limited to the sole resonant wavelength of the mode, and is not sufficient to understand the origin of the increase of the absorption integrated over a broad spectral range. In line with this, Yu et al. [17–19] have derived the analytical expression of the absorption by a resonance using the TDCMT. As their goal was to calculate the upper limit for absorption, they highlighted the impact of the spectral cross section of the resonances, yet the influence of the different coupling parameters on the absorption spectrum was not fully covered by their study. Consequently, we propose to address this issue by providing a more comprehensive analysis of the TDCMT model so as to facilitate the interpretation of the simulation and experimental results, and to propose design rules for more advanced solar cells including photonic nanostructures and resonances.

#183852 - $15.00 USD Received 4 Feb 2013; revised 17 Mar 2013; accepted 18 Mar 2013; published 22 Apr 2013

The first step consists in describing, in a low-absorbing spectral region, the optical properties of a PhC membrane, which is supposed to support a single mode without any assumption on its symmetry properties. This can be achieved thanks to the TDCMT using the same methodology and terminology as in [20], which gives the differential Eq. (1) describing the evolution of the field amplitude in a mode in the time domain:

$$\frac{da}{dt} = \left(j\omega_0 - \frac{1}{\tau_0} - \frac{1}{\tau_e} \right) a + \kappa_1 S_{+1}. \tag{1}$$

where a is the amplitude of the field in the mode, ω_0 is the resonant frequency of the mode, τ_e is the decay time of losses due to external coupling (in s), τ_0 is the decay time of losses due to absorption, and S_{+1} is the field amplitude of the incident light. This differential equation has to be coupled with the equations that apply to the coupling with the reflected and transmitted light:

$$\begin{aligned} S_{-1} &= -e^{-j\beta d} \kappa_2^* a \\ S_{-2} &= e^{-j\beta d} \left(S_{+1} - \kappa_1^* a \right). \end{aligned} \tag{2}$$

where S_{-1} is the field amplitude of the reflected light, S_{-2} is the field amplitude of the transmitted light, κ_1 is the coupling coefficient associated with the incident light and κ_2 is the coupling coefficient associated with the transmitted light. This is represented in Fig. 2(a), together with a schematic view of the photonic membrane (Fig. 2(b)).

As shown in [21], κ_1 and κ_2 can be related to τ_e via Eq. (3) by using τ_{e1} and τ_{e2} which are respectively the decay times on the front side and on the back side of the system:

$$\kappa_i = e^{-j\theta_i} \sqrt{\frac{1}{\tau_{ei}}} \qquad ; \qquad \frac{2}{\tau_e} = \frac{1}{\tau_{e1}} + \frac{1}{\tau_{e2}}. \tag{3}$$

In addition, it is noteworthy to highlight two coupling parameters. The first one is the τ_e/τ_0 ratio: high values for this ratio indicate that the intrinsic (or absorption) losses are dominating, whereas low values are obtained when external losses are prevailing. The second coupling parameter is the coupling anisotropy of the system denoted ζ. The latter is defined as follows:

$$\varsigma = \frac{\tau_{e_2}}{\tau_{e_1}}. \tag{4}$$

The parameter ζ can be infinite, as encountered in many devices involving a back reflector, but can also be adjusted within a sole absorbing layer by introducing a specific nano-patterning, for instance a double-layer 2D PhC [22] or by using patterns with non vertical sidewalls, e.g. like holes with radii changing along the membrane thickness [23].

#183852 - $15.00 USD Received 4 Feb 2013; revised 17 Mar 2013; accepted 18 Mar 2013; published 22 Apr 2013

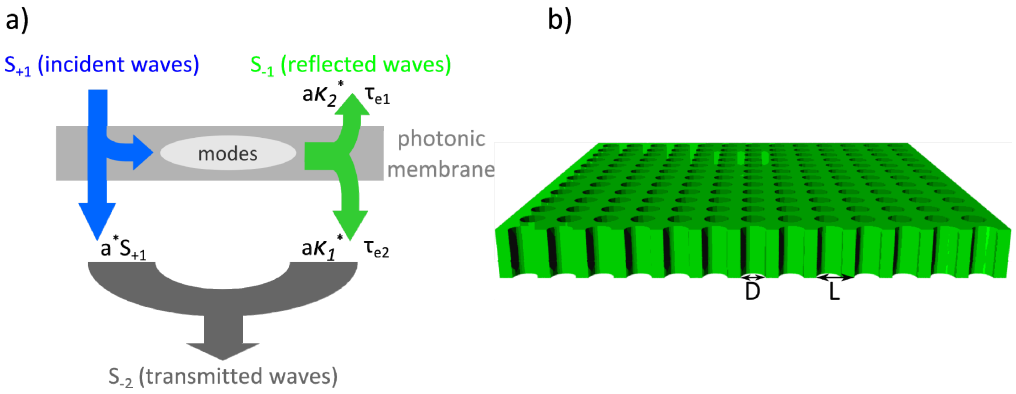

Fig. 2. TDCMT parameters used to describe the optical properties of the photonic membrane (a) and schematic view of the photonic crystal (b).

Using the harmonic steady-state hypothesis, one can solve Eq. (1) for any frequency (ω) detuned from the mode resonant frequency (ω_0) by ω-$\omega_0 = \delta\omega$:

$$a(\omega) = \frac{-\kappa_1 S_{+1}}{j\delta\omega - \frac{1}{\tau_0} - \frac{1}{\tau_e}}. \tag{5}$$

Starting from the above equations and introducing the expression of the field amplitude in the mode and of ζ, the reflection (r) and transmission (t) coefficients in field, can be expressed as follows:

$$\begin{aligned} \frac{S_{-1}}{S_{+1}} &= r = e^{-j\beta d}\, \frac{e^{-j(\theta_1-\theta_2)}}{\frac{\tau_e}{2}\sqrt{\left(\zeta + 2 + \frac{1}{\zeta}\right)}}\, \frac{1}{j\delta\omega - \frac{1}{\tau_0} - \frac{1}{\tau_e}} \\ \frac{S_{-2}}{S_{+1}} &= t = e^{-j\beta d} \left(1 + 2\, \frac{1}{\tau_e\left(1 + \frac{1}{\zeta}\right)}\, \frac{1}{\left(j\delta\omega - \frac{1}{\tau_0} - \frac{1}{\tau_e}\right)} \right). \end{aligned} \tag{6}$$

From Eq. (6), it is then possible to get the reflection (R) and transmission (T) coefficients in energy, as well as the resulting absorption (A = 1-R-T) as in (7);

#183852 - $15.00 USD Received 4 Feb 2013; revised 17 Mar 2013; accepted 18 Mar 2013; published 22 Apr 2013

$$R = rr^* = \frac{4}{\varsigma\left(1+\frac{1}{\varsigma}\right)^2\left[\left(\frac{\tau_e}{\tau_0}+1\right)^2+\tau_e^2\delta\omega^2\right]}$$

$$T = tt^* = \frac{4}{\left(1+\frac{1}{\varsigma}\right)}\frac{\frac{1}{\left(1+\frac{1}{\varsigma}\right)}-\left(\frac{\tau_e}{\tau_0}+1\right)}{\left(\frac{\tau_e}{\tau_0}+1\right)^2+\tau_e^2\delta\omega^2}+1 \tag{7}$$

$$A = 1-R-T = 4\left[\left(\left(\frac{\tau_e}{\tau_0}+1\right)^2+\tau_e^2\delta\omega^2\right)\left(1+\frac{1}{\varsigma}\right)\frac{\tau_0}{\tau_e}\right]^{-1}.$$

In the remainder of the paper, these expressions will be used in order to assess the influence of the τ_e/τ_0 ratio and of ζ on the width and on the highest achievable value of the absorption peak corresponding to the mode considered, and finally to determine the coupling conditions which maximize the integrated absorption of this isolated mode.

It can be first inferred from Eq. (7) that the expressions of R, (T-1) and A correspond to Lorentzian functions with a full width at half maximum (FWHM, denoted Γ) defined as:

$$\Gamma = 2\frac{\left(\frac{\tau_e}{\tau_0}+1\right)}{\tau_e}. \tag{8}$$

To illustrate Eq. (8), the FWHM was calculated for different τ_e/τ_0 ratios.

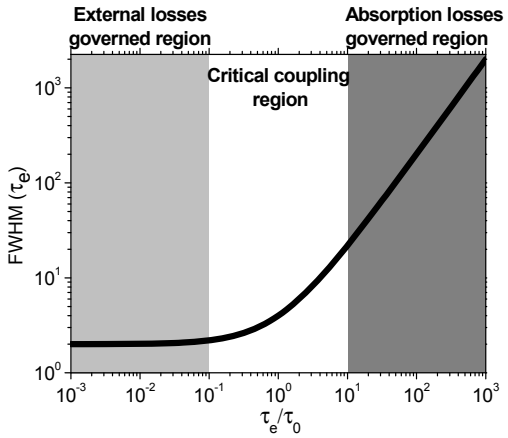

Fig. 3. FWHM (in τ_e units) of the R, T or A peaks as a function of τ_e/τ_0.

The results, gathered in Fig. 3, indicate that the FWHM increases together with the absorption losses, that is when τ_0 decreases. Conversely, the value of Γ is constant when the absorption losses are small compared to the external ones. As shown in [20], this can be expressed in terms of quality factors:

$$\frac{1}{Q_{tot}(\kappa)} = \underbrace{\gamma\times k}_{\substack{absorption\\losses}} + \underbrace{\frac{1}{Q_e}}_{\substack{esternal\\losses}}. \tag{9}$$

#183852 - $15.00 USD Received 4 Feb 2013; revised 17 Mar 2013; accepted 18 Mar 2013; published 22 Apr 2013

k being the extinction coefficient of the material considered proportional to τ_0^{-1}, γ a coupling coefficient and $Q_e = \omega_0\tau_e$. It can be noticed that due to the symmetry of Eq. (8) with respect to the parameters τ_0 and τ_e, the same curve as in Fig. 3 would be obtained by expressing the FWHM in τ_0 units.

In addition to the FWHM, another characteristic of the absorption peak impacting its integral is the maximum absorption value which can be attained. This occurs when the frequency is set to the one of the resonance of the mode, namely when $\delta\omega = 0$. After modifying Eq. (7) accordingly, one can compute $R_{\delta\omega = 0}$, $T_{\delta\omega = 0}$ and $A_{\delta\omega = 0}$ as a function of τ_0/τ_e for different ζ values (see Fig. 4(a)) or the other way around, i.e. as a function of ζ for different τ_e/τ_0 ratios (see Fig. 4(b)).

Firstly, Fig. 4(a) underlines the superposition of the reflection curves for ζ and $1/\zeta$. This results from the destructive interferences occurring between the transmitted and the reemitted waves since the mode is supposed to be at its resonance. For the symmetric membrane ($\zeta = 1$), it can be observed that a total reflection is obtained when the absorption losses are negligible. The value of the reflection is progressively decreasing when the coupling anisotropy increases.

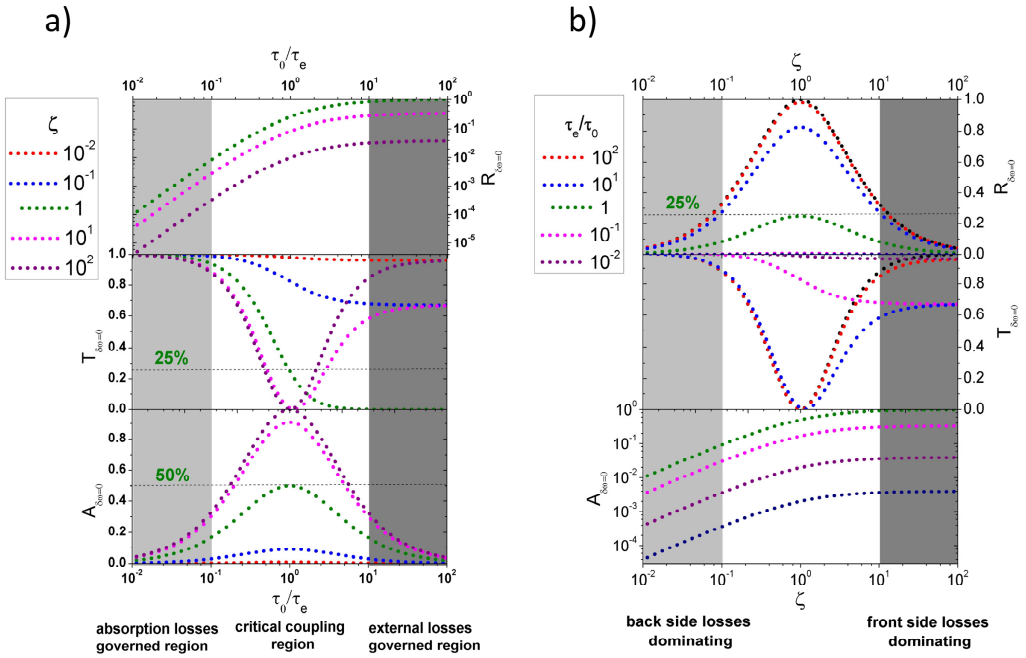

Fig. 4. Reflection, transmission and absorption of a single mode membrane, calculated as a function of τ_0/τ_e for different coupling anisotropy values (ζ) (a) and as a function of ζ for different τ_e/τ_0 ratios (b). Values are plotted at the resonant frequency.

Besides, small values of ζ (such as 10^{-2}) are associated with a high transmission ($T_{\delta\omega = 0}$ close to the unity whatever the τ_e/τ_0 ratio, see for instance Fig. 4(b)), since the front side coupling of the mode is weak and almost no energy can be injected in it, leading to both a low absorption and a low reflection. When the τ_0/τ_e ratio matches exactly the critical coupling conditions ($\tau_0/\tau_e = 1$), the transmission equals 25% for the symmetric membrane (same value as the one of the reflection) but tends to zero if ζ>10, which means that back side coupling can be neglected and that the absorption is then completely determined by the $R_{\delta\omega = 0}$ value.

Finally, this enables to understand the evolution of the absorption as a function of ζ and of the τ_0/τ_e ratio. It should be first emphasized that a maximum absorption is obtained when the intrinsic losses counterbalance the external ones, in other words, when the critical coupling conditions are fulfilled [14]. Under this condition ($\tau_0/\tau_e = 1$), the maximal absorption of the symmetric membrane is 50%. This value can be exceeded by increasing ζ. Indeed, after

#183852 - $15.00 USD Received 4 Feb 2013; revised 17 Mar 2013; accepted 18 Mar 2013; published 22 Apr 2013

introducing a strong coupling anisotropy (for instance $\zeta = 10^2$), a quasi-total absorption is achieved. Thus, it can be concluded that at the resonant frequency of the mode, a total absorption of the incoming light is possible provided that the best conditions on the coupling anisotropy (ζ close to 10^2) and on the τ_0/τ_e ratio ($\tau_0/\tau_e = 1$) are both achieved.

To go further, it should be precised that for most applications including photovoltaic devices or sensors, an optimization of the integrated absorption of the peak is required rather than just a maximization of $A_{\delta\omega = 0}$ for a targeted and single wavelength. Once again, it is possible to compute this integrated absorption (A_{int}) by considering the general expression of the integral of Lorentzian functions. A_{int} is then defined by $A_{\delta\omega = 0}$ and Γ, which depend directly on the coupling parameters ζ and τ_0/τ_e as seen previously.

$$A_{\text{int}} = A_{\delta\omega=0}\frac{\pi\Gamma}{2} = \frac{4\pi}{\left(\tau_e + \tau_0\right)\left(1+\frac{1}{\zeta}\right)}. \tag{10}$$

As an illustration of Eq. (10), A_{int} was calculated and plotted in Fig. 5 as a function of τ_0/τ_e, for different values of ζ. It can be noticed that increasing ζ from 10^{-2} to 10^2 enables to significantly increase the integrated absorption, regardless of the coupling regime considered. Moreover, for a given value of ζ, two distinct domains can be defined as regards the τ_e/τ_0 ratio, with a transition occurring around the critical coupling conditions. More precisely, A_{int} rises as τ_e/τ_0 decreases and eventually converges towards an optimal value when the external losses are dominating. As it was highlighted in [19], the spectral cross-section of a single resonance is maximized in this over-coupling regime. Furthermore, one can observe in Fig. 5 that a −3dB cutoff takes place precisely at critical coupling. This means that increasing the external losses so that they can equal the intrinsic ones is a must, and strengthening them to overcome the absorption losses is a plus.

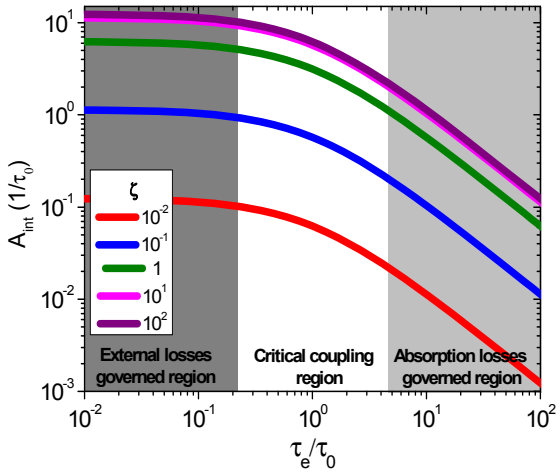

Fig. 5. Integrated absorption (in τ_0^{-1} units) calculated for different coupling parameters.

So as to achieve a broadband absorption enhancement, the goal is not only to select a mode operating in the over-coupling regime, but also to fill properly the targeted spectral range with a collection of such modes. A generalization of Eq. (10) to a set of N non-overlapping modes enables to calculate the total integrated absorption $A_{int,tot}$:

$$A_{\text{int},tot} = 4\pi\sum_{i=1}^{i=N}\frac{1}{\left(\tau_{e,i} + \tau_{0,i}\right)\left(1+\frac{1}{\xi_i}\right)}. \tag{11}$$

#183852 - $15.00 USD Received 4 Feb 2013; revised 17 Mar 2013; accepted 18 Mar 2013; published 22 Apr 2013

This formula describes corrugated absorbing layers such as PhC membranes in regions where the spectral range between consecutive modes is large compared to their linewidth. To illustrate the discussion above, let us consider two examples of absorbing PhC structures. The first example consists of a 100nm thick a-Si:H layer, patterned as a 1D PhC, with a lattice parameter L = 450nm, and 146nm wide air slits. Its absorption spectrum is simulated using Finite-Difference Time-Domain (FDTD) simulations, considering normal incidence illumination, with a Transverse Magnetic (TM) polarization. The spectrum, plotted in Fig. 6, exhibits a single peak which corresponds to a resonant mode of the PhC, with a quality factor of 30, as determined with a harmonic inversion code [24]. The critical quality factor Q_c, defined as $n/2\kappa$, where n is the refractive index of the absorbing material, is also indicated on the graph. One can note that the quality factor of the resonant mode is almost equal to Q_c at the corresponding wavelength, 640nm. This explains that around 50% absorption is achieved at this wavelength. One should note that even for a vertically symmetric membrane, the absorption reached in this spectral region is not limited to 50% due to an additive absorption law [20]. Indeed, the absorption of this resonance can be added to the background absorption emerging from Fabry-Pérot resonances, possibly combined to the absorption of the surrounding resonances originating from the patterning, as will be shown in the next example.

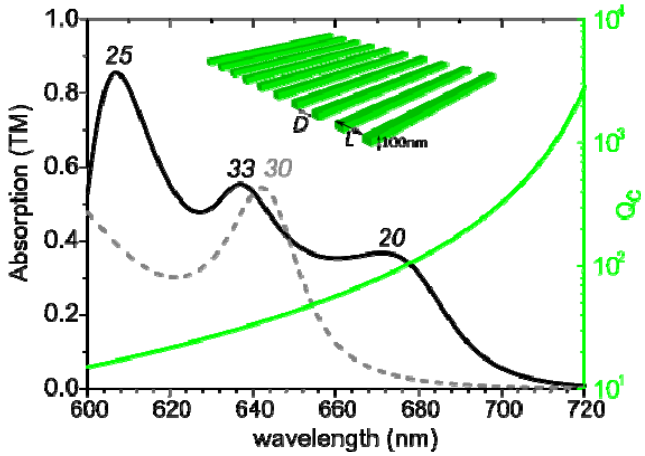

Fig. 6. Simulated absorption spectra for two 1D PhC structures. The dashed line corresponds to an unoptimized structure with L = 450nm, D = 146nm. The solid line corresponds to an optimized structure, with L = 597nm and D = 197nm. The quality factor of each absorption peak is indicated in italic. The green line corresponds to, Q_c. The computed structure is schematized in the inset.

We investigate a second case in which the geometrical parameters of the PhC (period L and air slit width) are optimized. This leads to L = 597nm, and D = 197nm. The corresponding absorption spectrum is also shown in Fig. 6; the integrated absorption is increased from 19.6% to 36.7%. It clearly appears on the spectrum that this increase can be accounted for by the creation of two additional resonances surrounding the previous one. While the resonances located at around 607nm and 637nm correspond to critical coupling conditions, it should be noted that the one at 671nm lies in its over-coupling regime (Q_c = 80 at λ = 671nm, to be compared to the value of 20, computed in the case of this PhC structure). This results in a broad absorption enhancement close to the a-Si:H bandgap.

In summary, we have analyzed the coupling properties of resonant modes, and we have presented their potential to optimize their peak and integrated absorption in a low-absorbing spectral region. In this context, it was first concluded that the coupling anisotropy of the system should be maximized as much as possible. A second requirement was to bring the external losses at least at the critical coupling conditions. The goal is then to broaden the modes so as to reach the over-coupling regime, and to fill properly the spectral region with a

#183852 - $15.00 USD Received 4 Feb 2013; revised 17 Mar 2013; accepted 18 Mar 2013; published 22 Apr 2013

collection of modes, in order to optimize the resulting absorption enhancement. A general objective of the design is then to generate additional optical resonances which are strongly coupled to the radiative continuum. This can be achieved simply by changing the main parameters of the PhC, or, more efficiently, by including a multiple periodicity, or even a controlled degree of disorder, in a simply periodic pattern. Example of such structures can be found in the recent literature [25–27]. In this section, the results were illustrated in the case of a simple 1D PhC made of a-Si:H. However, they are also valid in the case of a full solar cell stack patterned as a 2D PhC or more complex structures. In particular, the computed spectrum displayed in Fig. 1(b), in the case of the optimized 2D PhC solar cell, illustrate the positive impact of multiple damped optical resonances.

In the case of crystalline silicon (c-Si) thin film solar cells, like those discussed in [28–30], one can draw similar conclusions. However, as the resonances are then very densely packed, Eq. (7) cannot be applied in a straightforward way: the interplay between the optical modes is hardly taken into account by this simple analytical model. It remains that in this practical case, as the thickness of the c-Si layer is necessarily much higher than in the a-Si:H case, since the absorption coefficient is lower. Then, the PhC membrane may support a much higher spectral density of optical resonances, with increased quality (Q) factors. The optimization process then tends to select such densely packed modes, close to the critical coupling conditions; this leads to a higher integrated absorption.

4. Angular acceptance of a-Si:H based photonic crystal assisted solar cells

Additionally to the necessary optimization of the absorption efficiency, any photonic engineering strategy for photovoltaics should be compatible with a reasonable angular acceptance. Although relying on optical resonances, absorbing PhC structures bring a key intrinsic advantage: these modes correspond to relatively flat dispersion curves. Such optical resonances are then expected to exhibit relatively stable properties with regards to the angle of incidence. Additionally, as it has been highlighted in the last section, the behavior of a single PhC layer relies on several optical modes; even if their behavior is modified with the incidence angle, it may be expected that the impact of these modifications could be globally compensated when integrated over a broad spectrum. Lastly, in the case of PhC structures, the coupling of light at normal incidence is prohibited for specific symmetries of modes [31]. As a result, the integrated absorption may be increased while the incidence angle is tilted with regards to normal incidence. In order to assess the positive impact of these specific properties of PhC Bloch mode resonances, the integrated absorption has been calculated by Rigorous Coupled Wave Analysis (RCWA), for two different structures, between 300 and 720nm, considering the AM1.5G solar irradiance.

Figure 7(a) displays the integrated absorption evolution in the case of an optimized absorbing 2D PhC constituted of a 100nm a-Si:H layer, with a lattice parameter L = 300nm, and holes diameter of 240nm [15]. It clearly appears that the integrated absorption is much higher in the case of the PhC, for all incidence angles up to 80°. While the integrated absorption is increased by a factor of 2 at normal incidence, this factor is in excess of 3 at 80°. Moreover, the integrated absorption increase is clearly visible in the PhC case, when the incidence angle is increased from 0 to 10°. All these remarks illustrate the properties and confirm the tendencies discussed in the beginning of this section.

The computed data displayed in Fig. 7(b) corresponds to the structure schematized in Fig. 1(a): an a-Si:H solar cell stack patterned as a 2D PhC, with optimized integrated absorption (L = 380nm, and D = 237.5nm). In this second situation, similar results are obtained: a slight absorption increase from 0 to 10° for the patterned stack and a higher absorption at every angle in the case of the PhC, compared to the unpatterned reference. However, it turns out that the absorption increase is lower in this stack, compared to the sole patterned a-Si:H layer. The reason is that the presence of the back electrode and of the top ITO layer lead to a substantial absorption increase of the unpatterned stack. Still, the integrated absorption in a-Si:H is only decreased from 65.7% to 60%, while the angle of incidence is increased up to 55°.

#183852 - $15.00 USD Received 4 Feb 2013; revised 17 Mar 2013; accepted 18 Mar 2013; published 22 Apr 2013

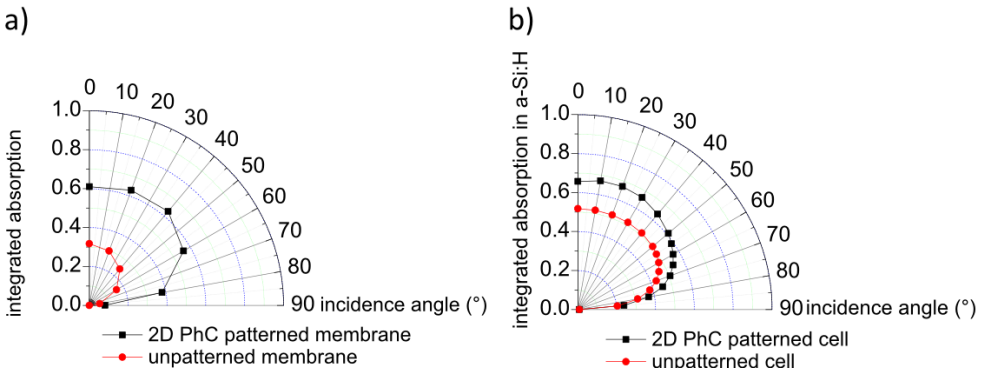

Fig. 7. Simulated integrated absorption for an a-Si:H unpatterned and 2D PhC patterned layer (a) and for the unpatterned and 2D PhC patterned solar stack (b). The solar cell stack corresponds to the structure schematized in Fig. 1(a). In both cases, the absorption is integrated from 300 to 720nm, considering an AM1.5G solar distribution.

Finally, Fig. 8(a) exhibits measured absorption spectra obtained with an integrating sphere. In this case, a solar cell stack was deposited, and 2D PhC structures were patterned using laser interference lithography and reactive ion etching. Details of the processes can be found in [14]. The PhC geometrical parameters were relatively far from the optimal situation, since L = 600nm, and D = 350nm. The spectra measured at angles of incidence α between 10 and 50° exhibit a relatively stable behavior. Indeed, there is no global decrease of the overall integrated absorption as underlined in Fig. 8(b). More precisely, it clearly appears that the wavelength of the resonant modes is tuned for increasing angles, and that there is a compensation phenomenon between the peaks which appear or disappear with a changing angle of incidence.

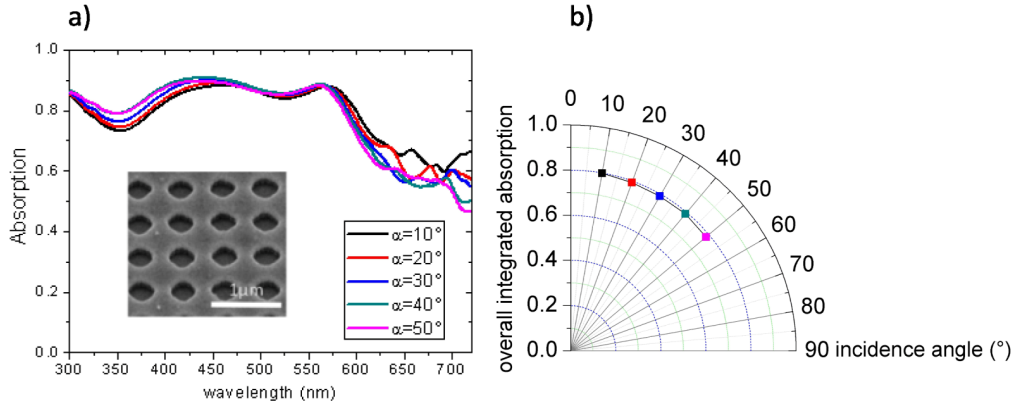

Fig. 8. Absorption spectra measured for an a-Si:H based solar cell stack, patterned as a 2D PhC (with L = 600nm and D = 350nm). Measurements are performed in an integrating sphere, with angles of incidence from 10 to 50° (a scanning electron micrograph of the patterned solar cell stack is shown in the inset (a). The overall integrated absorptions calculated from those spectra are also reported (b).

5. Conclusion

Patterning a silicon-based thin film solar cell as a 2D PhC enables a substantial increase of the absorption efficiency. In the case of a device including a 100nm thick a-Si:H p-i-n junction, and all the necessary layers to collect the electrical carriers, the relative increase is up 27%. This is achieved by a simple patterning of the stack as a square lattice of air holes. To further increase this absorption efficiency, it is necessary to refine the design of the photonic

#183852 - $15.00 USD Received 4 Feb 2013; revised 17 Mar 2013; accepted 18 Mar 2013; published 22 Apr 2013

structure and to perform optical mode engineering. To reach this goal, we have introduced a method based on a TDCMT analysis. Using this method, it is possible to evaluate, and maximize the absorption around a given wavelength, which can be useful for indoor photovoltaics, or down-conversion structures for third generation solar cells. It is also possible to optimize the integrated absorption in a given wavelength range, increasing the spectral density of optical modes, and generating optical resonances operating in the over-coupling regime. Such resonances can be generated by a careful choice of the PhC structure parameters, or, more efficiently, by using a more complex unit cell, partially etched photonic structures or patterns with a controlled disorder. In the case of an absorbing layer with a thickness in the micrometer range, the spectral density of optical modes can be further increased, with the possibility to use resonances closer to the critical coupling conditions, with lower optical losses.

Another key characteristic of PhC resonances is that they enable a particularly high angular acceptance. Using RCWA simulations, we have shown that the integrated absorption in the a-Si:H active layer of a patterned solar cell stack is only decreased from 65.7% to 60%, while the incidence angle is increased from 0 to 55°. This excellent stability has been confirmed by optical measurements, for angles of incidence up to 50°.

Acknowledgments

This work was supported by Orange Labs Networks contract 0050012310-A09221. Ounsi El Daïf, from IMEC, is acknowledged for performing the angular acceptance measurements. Pere Roca i Cabarrocas, from LPICM, is acknowledged for the deposition of the solar cell stack used in section 4, and for fruitful discussions.

#183852 - $15.00 USD Received 4 Feb 2013; revised 17 Mar 2013; accepted 18 Mar 2013; published 22 Apr 2013